Available online at www.sciencedirect.com
SCIENCE DIRECT®
Biomaterials 25 (2004) 5753–5762
Biomaterials
www.elsevier.com/locate/biomaterials

Functional cardiac cell constructs on cellulose-based scaffolding

Emilia Entcheva[a,b,*], Harold Bien[a], Lihong Yin[a], Chiung-Yin Chung[a], Melissa Farrell[a], Yordan Kostov[c,*]

[a] Department of Biomedical Engineering, Stony Brook University, HSC T18-030, Stony Brook, NY 11794, USA
[b] Department of Physiology and Biophysics, Stony Brook University, Stony Brook, NY 11794, USA
[c] Department of Chemical and Biochemical Engineering, University of Maryland, Baltimore County, USA

Received 31 July 2003; accepted 20 January 2004

Abstract

Cellulose and its derivatives have been successfully employed as biomaterials in various applications, including dialysis membranes, diffusion-limiting membranes in biosensors, in vitro hollow fibers perfusion systems, surfaces for cell expansion, etc. In this study, we tested the potential of cellulose acetate (CA) and regenerated cellulose (RC) scaffolds for growing functional cardiac cell constructs in culture. Specifically, we demonstrate that CA and RC surfaces are promoting cardiac cell growth, enhancing cell connectivity (gap junctions) and electrical functionality. Being optically clear and essentially non-autofluorescent, CA scaffolds did not interfere with functional optical measurements in the cell constructs. Molding to follow fine details or complex three-dimensional shapes are additional important characteristics for scaffold design in tissue engineering. Biodegradability can be controlled by hydrolysis, de-acetylization of CA and cytocompatible enzyme (cellulase) action, with glucose as a final product. Culturing of cardiac cells and growth of tissue-like cardiac constructs in vitro could benefit from the versatility and accessibility of cellulose scaffolds, combining good adhesion (comparable to the standard tissue-culture treated polystyrene), molding capabilities down to the nanoscale (comparable to the current favorite in soft lithography—polydimethylsiloxane) with controlled biodegradability.
© 2004 Elsevier Ltd. All rights reserved.

Keywords: Cardiac tissue engineering; Cardiomyocyte; Cell culture; Cellulose; Fluorescence; Scaffold

1. Introduction

Cell culture and tissue engineering can benefit from the use of versatile cost-effective scaffold materials that can be modified easily. Desired biomaterial modifications usually include the introduction of controlled porosity [1,2]; the design of three-dimensional structures [3–5]; and surface modifications [6,7] for better cell packing and control of cell network architecture. These features, combined with requirements for biocompatibility and biodegradability (if intended for implantation), constitute the characteristics of the ideal biomaterial for tissue engineering. Different polymer classes are currently under testing for providing the optimal scaffolding in cell and tissue growth [8].

Cellulose is the most abundant naturally occurring polysaccharide formed out of glucose-based repeat units, connected by 1,4-beta-glucosidic linkages. Cellulose and its derivatives are widely used as tough versatile materials. Cellulose nitrate, cellulose acetate (CA) and cellulose xanthate (rayon) can be easily molded or drawn into fibers for textile applications, for designing composite materials (safety glass), as thermoplastics etc. Unlike starch (very similar glucose-based structure but with alpha linkages), cellulose-based materials have very low water solubility, therefore allowing for better control over scaffold design. Hydrogen bonds from the hydroxyl groups, holding the cellulose chains together, account for the high degree of crystallinity, low solubility and poor cellulose degradation in vivo. The presence of amorphous regions can increase biodegradability in tissue [9]. Lowering the crystallinity and

*Corresponding authors. Department of Biomedical Engineering, Stony Brook University, HSC T18-030, Stony Brook, NY 11794, USA. Tel.: +1-631-444-2368; fax: +1-631-444-6646.
E-mail addresses: emilia.entcheva@sunysb.edu (E. Entcheva), kostov@umbc.edu (Y. Kostov).

0142-9612/$ - see front matter © 2004 Elsevier Ltd. All rights reserved.
doi:10.1016/j.biomaterials.2004.01.024

augmenting the hydrophilicity of cellulose-based materials are known approaches to improve their biodegradability in vivo.

Biomaterials based on cellulose and its derivatives have been used as: (1) hemodialysis membranes [10,11]; (2) diffusion-controlling membranes and membrane-carriers for enzyme immobilization in biosensors [12–14]; (3) coating materials for drugs and drug-releasing scaffolds [15,16]; (4) in vitro hollow fibers perfusion systems [17,18] and in other biomedical applications. More recently, several studies report the applicability of cellulose-based materials for culturing cells and for implantation. Examples include bone regeneration [19–21], hepatocyte culturing for an artificial liver [8,22–24], expansion of progenitor hematopoetic cells in culture [25] and suppression of matrix metalloproteases (MMPs) action in wound healing [26,27]. In vitro and in vivo applications of cellulose-based materials have demonstrated only negligible foreign body and inflammatory response reactions [9,20,28], thus they are considered biocompatible. The introduction of small amount of cationic groups can further improve tissue compatibility of cellulose-based materials [9].

Previous biomedical applications of cellulose-derived materials suggest their potential use as general supporting and guiding structures for cell culture and possibly for reparative tissue engineering. In this study we demonstrate the utility of CA and regenerated cellulose (RC) for engineering electromechanically functional cardiac muscle constructs in vitro. This biocompatible polymer with excellent shape-conforming properties for three-dimensional scaffold design could effectively address the structural complexity of the cardiac muscle and the need for perfusion structures in culture.

2. Materials and methods

2.1. Cellulose acetate and regenerated cellulose scaffolds

CA scaffolds for cell growth were prepared by mixing 1 g CA with 39.8% acetyl content (Aldrich Chemical, Milwaukee, WI) and 20 ml of spectroscopic grade acetone (Adrich) to obtain a clear solution, which was then dried slowly (covered overnight) to form thin (50–200 μm) optically clear durable membranes. Partial hydrolysis and de-acetylization were applied to the CA scaffolds using 100 mM NaOH for different time intervals (6 and 24 h) at different temperatures (25°C and 60°C) to obtain RC. It is known that such treatment results in some increase of the nanoscale porosity [29]. The molding potential of CA was tested by casting the polymer from the surface of fine optical gratings (30,000 lines/in, i.e. 850 nm per line) or by fabricating wavy microscale fibers or three-dimensional grooved topographies by casting onto micromachined surfaces. Fig. 1 shows examples of micro-scale feature molding using CA.

Control surfaces for cell growth included culture-treated polystyrene wells (VWR, West Chester, PA) (PS), standard glass coverslips No. 1 (VWR) (GL), and polydimethylsiloxane (PDMS) (Sylgard 184 from Dow Corning, Midland, MI). PDMS membranes were prepared in the usual ratio of 1:10 of curing agent to elastomer and baked for 2 h at 60°C. All scaffolds were sterilized in ethanol or using UV light.

2.2. Primary culture of cardiac myocytes and fibroblasts

Cardiac cells were obtained from neonatal Sprague-Dawley rats, 2–4 days after birth, as described previously [30,31]. Briefly, enzymatic treatment with trypsin (at 1 mg/ml, overnight, at 4°C), followed by collagenase (at 1 mg/ml, repeated treatment at 37°C) (Worthington Biochemical, Lakewood, NJ) was applied to digest the heart ventricles of 9–12 pups at a time. Through a 45 min pre-plating procedure, cardiac fibroblasts (FB), which attach first, were separated from cardiac myocytes (CM). Non-dividing CM were plated on the desired surfaces immediately post-dissociation at 400×10^3 cells/cm^2, while moderately proliferating FB were trypsinized (0.05% trypsin and 0.5 mM EDTA, Gibco, Grand Island, NY) 4–6 days later and re-plated at 20×10^3 cells/cm^2; FB from 1 to 4 replatings were used. The examined surfaces were pre-incubated for 1.5 h with fibronectin at 50 μg/ml (BD Biosciences,

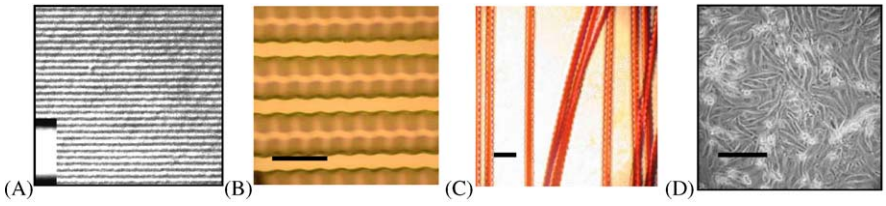

Fig. 1. Microscale shaping of CA. Microphotograph (A) shows actual CA molding out of a master optical grating with 850 nm feature periodicity; (B) is a phase contrast image of a CA sample with microgrooved sinusoidal channels; (C) shows wavy three-dimensional CA fibers, manufactured from microfabricated surfaces, red ink was mixed with the polymer to increase contrast. Phase contrast photograph of closely packed cardiac myocytes grown on RC is shown in (D). Scale bar is 10 μm in A; 100 μm in B, and 200 μm in C and D.

Franklin Lakes, NJ). Both cell types were maintained at 37°C with 5% CO_2 in medium 199 (Gibco) supplemented with 2% fetal bovine serum (Gibco).

2.3. Fluorescent cell labeling, cell adhesion and cell viability assays

For structural characterization, cells were fixed at days 2–7 after plating in 3.7% formaldehyde and permeabilized with 0.02% Triton-X 100. Cell cytoskeleton was fluorescently stained with phalloidin–Alexa Fluor 488 (Molecular Probes, Eugene, OR) for F-actin. Nuclei of fixed cells were labeled with TOTO-3 (Molecular Probes) for confocal imaging or DAPI otherwise; live cells nuclei were labeled with SYTO-16 (Molecular Probes) at 0.5 μM for 5 min. Gap junctional protein (Connexin 43) was detected by immunocytofluorescence using a primary rabbit anti-mouse Cx43 affinity-purified polyclonal antibody (Chemicon, Temecula, CA), combined with a secondary Alexa Fluor 488 goat anti-rabbit IgG (Molecular Probes) as a fluorescent probe.

Fibroblast proliferation and retention to the scaffolds was quantified over a 12 day period using a cell titer assay CellTiter 96© AQueous One Solution (Promega, Madison, WI). Cells on each scaffold were treated with 50 μl reagent for 4 h, and a solution sample was taken for analysis. CellTiter 96© contains a tetrazolium compound (MTS), that is bioreduced by metabolically active cells to produce a colored formazan product, which was measured by absorbance at 490 nm, subtracting a background of 650 nm. A calibration curve of known cell number versus optical density was prepared to determine cell number on the scaffolds.

Cell viability was assessed after one week in culture using a combined propidium iodide (Molecular Probes) at 2 μg/ml for 2 min and SYTO-16 at 0.5 μM for 5 min staining. These two dyes competitively stain cell nuclei, with SYTO-16 being membrane permeable and labeling live cells, while propidium iodide only labels the nuclei of cells with compromised membrane integrity. Fluorescence was collected at the corresponding wavelengths for the two dyes, and the percentage of viable cells was quantified by the ratio of propidium iodide to SYTO-16 stained nuclei.

2.3.1. Structural fluorescence imaging and morphological analysis

Structural fluorescence imaging was performed using a confocal laser-scanning microscope BioRad Radiance 2000 with a 60× oil-immersion objective (N.A. 1.4), or an inverted fluorescence microscope Nikon TS100 with a 40× objective (N.A. 0.95) and a microscope-attached Nikon Coolpix 995 digital camera. All images were properly scaled. Automated analysis of Connexin-43 immunocytochemistry images was conducted using the Image Processing Toolkit in Matlab (Mathworks) using *granulometry* [32], as described previously [33]. Statistical analysis was performed using a two-sided *t*-test.

2.4. Dynamic fluorescence imaging of action potentials and intracellular calcium in cardiomyocyte networks

Action potentials (V_m) and intracellular calcium transients ($[Ca^{2+}]_i$) in cardiac myocytes were measured optically using voltage- and calcium-sensitive dyes, which respond by instantaneous change in fluorescence to changes in V_m or $[Ca^{2+}]_i$. During the experiments in live cells, the scaffolds were transferred to a custom made experimental chamber with embedded Platinum electrodes, and the cells were superfused with normal Tyrode's solution (in mM): 135 NaCl, 5.4 KCl, 1.8 $CaCl_2$, 1 $MgCl_2$, 0.33 NaH_2PO_4, 5 HEPES, 5 glucose, adjusted to pH 7.4 with NaOH, at 23±2°C. For V_m measurements, the cells were incubated with the voltage-sensitive dye di-8-ANEPPS (Molecular Probes) for 5 min. Same cells were co-stained for 20 min with Fura-2 for $[Ca^{2+}]_i$ assessment. *Microscopic* measurements were performed using a Nikon Eclipse TS100 microscope, with a 20× S Fluor objective (N.A. 0.75) in epi-illumination using a photomultiplier tube (PMT, Electron Tubes Lmtd, UK) at a sampling rate of 1 kHz. V_m and $[Ca^{2+}]_i$ measurements were conducted sequentially at the same spatial location. Calcium was measured ratiometrically by exciting at 380 and 365 nm (the isobestic point). Intensity fluorescence measurements of V_m were conducted with excitation at 535 nm.

Macroscopic measurements for resolving propagation of electrical activity in multicellular preparations were performed using an intensified CCD camera (DAGE MTI, Michigan City, IN) and a custom-built optical setup, as described previously [33]. Propagation maps were constructed by plotting activation times over the imaged space.

2.5. Cellulase treatment

Cellulase is a common name for a group of enzymes that attacks 1,4-beta-glucosidic bonds, thereby selectively breaking cellulose into smaller length chains down to its glucose repeat units. For RC scaffold degradation tests prior to cell plating, we used cellulase (a mixture of endoglucanase, exoglucanase (cellobiohydrolase) and a β-glucosidase) from Trichoderma reesei (Sigma, St. Louis, MO), treating each scaffold with about 70 enzyme units over the course of 24 days at 37°C, pH 7.2. Cellulase compatibility with cardiac cells was tested by treating cell-plated RC scaffolds with variable enzyme solutions (23, 46 or 92 units per scaffold) for

24 h at 37°C (culture medium), added at day 4 in culture.

3. Results

3.1. Microscale shaping of cellulose acetate scaffolds

Cellulose-based materials, particularly the CA form, can be easily molded into complex three-dimensional shapes (as exemplified by commercially available hollow microfibers, for example) and are able to follow micro- and nano-scale surface features (Fig. 1). We show a CA cast in Fig. 1A with sub-micron features, as well as examples of sinusoidal microgrooves in Fig. 1B, and high-surface area wavy cellulose microfibers in Fig. 1C, prepared in our lab.

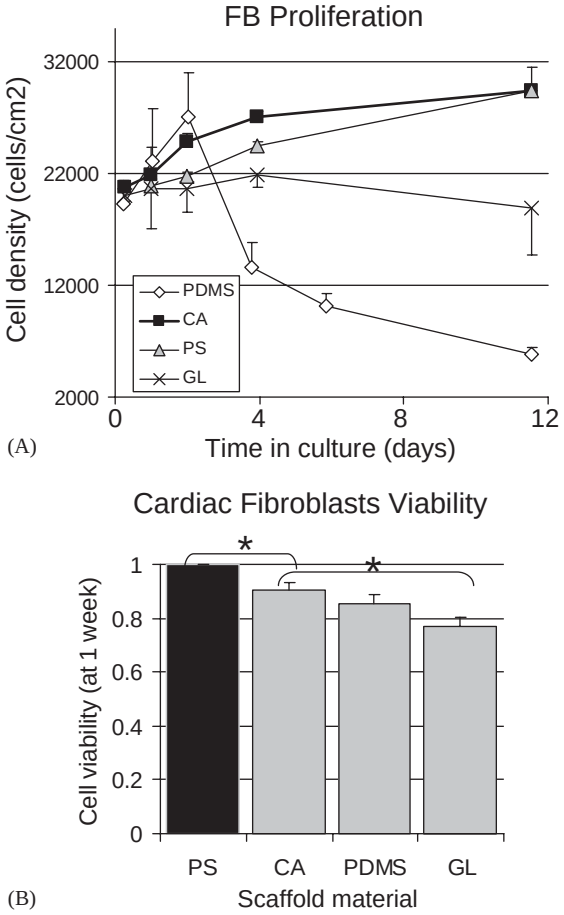

Fig. 2. Cardiac fibroblasts on cellulose scaffolds: (A) Proliferation of primary cardiac fibroblasts (FB) was assessed at days 0, 1, 2, 4, 12 in culture. Culture-treated polystyrene (PS) was used as a standard; cellulose acetate (CA); PDMS and glass (GL) were examined. Shown are data (mean ± S.E.M.). CA demonstrates a similar proliferation trend as the standard PS, while cells on GL, and particularly PDMS, show a downward trend after day 2 in culture. (B) Viability of primary cardiac fibroblasts was assessed after 1 week in culture; data are presented as (mean ± S.E.M). CA exhibited lower cell viability than PS but higher viability than GL ($p < 0.05$, *) and PDMS.

3.2. Proliferation and viability of cardiac fibroblasts on CA surfaces

Fig. 2A demonstrates the promotion of proliferation of cardiac fibroblasts and their good retention on CA scaffolds over a 12 day period. A similar trend, but with a slower rate of rise, was observed for tissue culture-optimized PS surfaces. In contrast, cells on glass coverslips and PDMS peaked in number at approximately 2–4 days in culture, and then followed a downward trend, particularly for PDMS surfaces. Curves were based on 10, 18, 40 and 17 cultures for PS, GL, PDMS and CA, respectively, with 2–9 scaffolds per time point. Fig. 2B shows viability of primary cardiac fibroblasts assessed after 1 week in culture. CA exhibited lower cell viability than PS but higher viability than GL ($p < 0.05$) and PDMS; more than 500 cells were analyzed per case. Overall, adhesion and preservation of cell viability on protein-coated CA surfaces were on par with the current standard in cell culture, polystyrene.

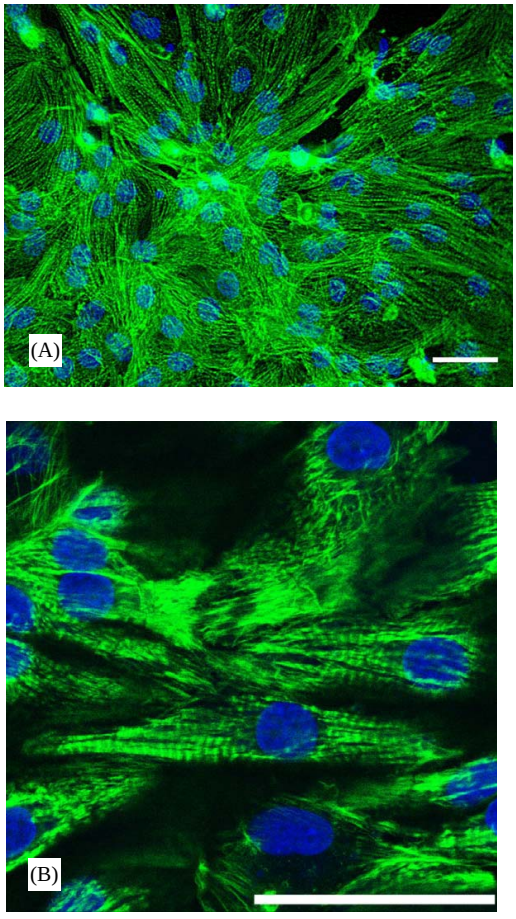

Fig. 3. Cytoskeleton maturity in CA-grown myocytes. A and B shows well-packed myocytes at two different scales. F-actin is fluorescently labeled in green, nuclei—in blue using DAPI (A) or TOTO-3 (B). Scale bar is 50 μm.

3.3. Structure and electromechanical function of cellulose-grown cardiomyocyte networks

A distinct structural feature of the cytoskeleton of mature cardiac myocytes is the periodic myofibril organization, composed of individual contractile units about 2 μm long—the sarcomeres. This signature structural characteristic of differentiated muscle cells is often missing in culture-grown neonatal cardiomyocytes. However, we found that cellulose scaffolding in its two varieties—CA and RC—consistently promoted mature sarcomere organization, as shown at two different magnifications in representative cytoskeletal images of F-actin (Fig. 3). Additionally, Fig. 3A demonstrates high packing and confluency for CM, as seen for FB.

Intercellular communication and effective transmission of electrical signals in cardiomyocytes relies on gap junctional proteins; Connexin 43 (Cx43) is the major gap junctional protein in ventricular cells. Immunofluorescent confocal images of Cx43 distribution in monolayers of CM, grown on CA and on glass coverslips are shown in Figs. 4A and B, respectively; Fig. 4C shows CM grown on microgrooved three-dimensional CA with 100 μm groove spacing and 10 μm groove depth. The fluorescent labeling of Cx43 produces bright spots, whose size and density could be directly linked to the extent of cell–cell communication [34,35]. Fig. 4D summarizes our quantification of gap junctions for identical areas covered by CM on CA (5 cultures) scaffolds and on glass coverslips (3 cultures) as controls. An overall increase of gap junction size and density was observed for CA-grown cells vs. glass-grown myocytes, with two of the gap junction size categories (0.45 and 1.85 μm^2) showing statistical significance ($p < 0.05$). Note that these observations were not brought about by a simple difference in cell density between CA and GL ($p > 0.22$). These results likely indicate overall improved cell–cell communication, but further functional characterization is needed.

To test electromechanical competence of the engineered constructs, we used dynamic optical measurements with voltage- and calcium-sensitive dyes. Figs. 5B and C (right) schematically outline the components in our fluorescence measurement system, built around an inverted microscope (5B) or a tandem-lens optical

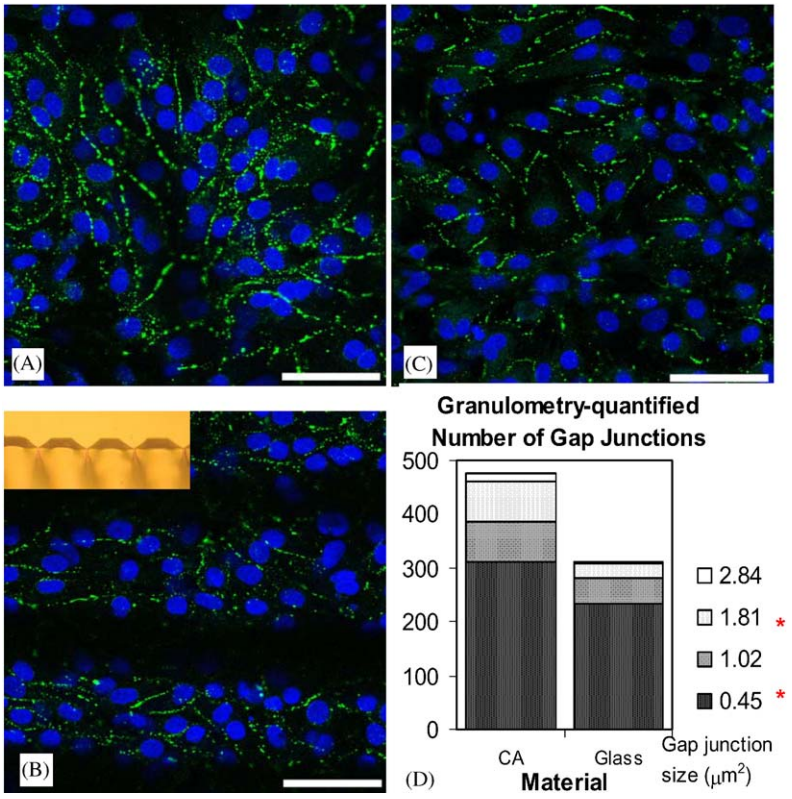

Fig. 4. Cell-to-cell communication (gap junctions) in CA-grown myocytes (A and B), compared to cells grown on glass coverslips (C). Cells in A and C were plated on a flat surface; while a CA scaffold in B had periodic three-dimensional undulations; inset shows a cross-section of the scaffold surface. Confocal images were obtained after immunolabeling for Connexin 43 (green) and TOTO-3 labeling of nuclei (blue). Scale bar is 50 μm. D. Granulometry-based quantification of gap junctional size distribution on CA and glass from confocal images (like A and C). Increase in the overall number of gap junctions per area was observed on CA, plus a statistically significant difference between CA and glass for 2 gap junction size categories, indicated by a star.

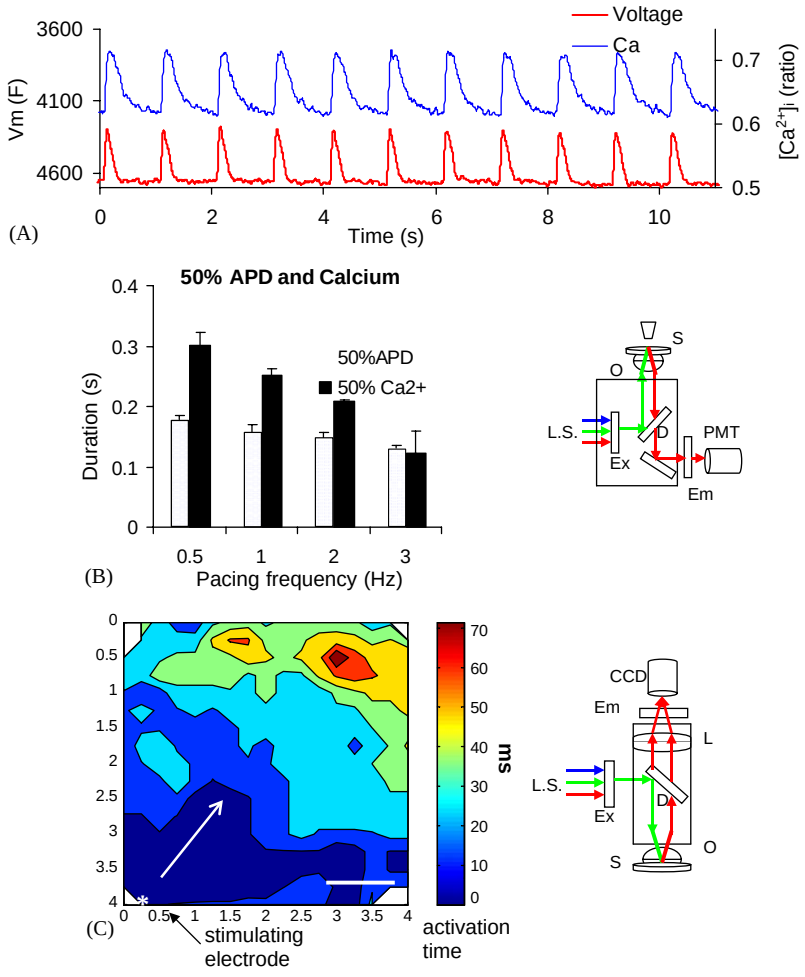

Fig. 5. Electromechanical functionality of cellulose-grown excitable cell networks (A) Optically recorded action potentials (V_m) and calcium transients ($[Ca^{2+}]_i$) in CA-grown myocytes during external 1 Hz pacing, 5 V/cm. Cells were co-stained with voltage- and calcium-sensitive fluorescent dyes; (B) Restitution properties, i.e. response to different pacing frequencies (0.5–3 Hz), data are presented as (mean ± S.D.); (C) Propagation map of action potentials, demonstrating cardiac syncytium behavior on a CA scaffold. The map shows activation times in color (from 0–70 ms) in response to a point electrode at the lower left corner; scale bar is 1 mm. The optical configurations, shown on the right of B and C, were used to obtain the fluorescence measurements of electrical activity in the samples (S) at the micro—(A, B) and macroscale (C), including a light source (L.S.), an objective lens (O), an excitation filter (Ex), an emission filter (Em), a dichroic mirror (D), a secondary lens (L), a photomultiplier tube (PMT) and an intensified CCD camera (CCD).

configuration (5C). Representative traces of action potentials and calcium transients at 1 Hz pacing are shown in Fig. 5A. Normal frequency dependence (restitution of V_m and $[Ca^{2+}]_i$) at 50% duration is demonstrated in Fig. 5B using samples from 3 cultures. Electrical activity, induced by a stimulating point electrode, propagated in macroscopically homogeneous patterns at conduction velocities 6–15 cm/s at room temperature. A typical propagation map from a CA-grown cell network, paced at 1 Hz is shown in Fig. 5B, with point stimulation at the left bottom corner, and colors corresponding to the times of activation. In the shown map, times of activation were extracted from the action potential traces at 256 spatial locations (16×16) covering a $0.4 \times 0.4\,cm^2$ area. Overall, excitability of cellulose-grown cardiomyocytes was normal and maintained in culture.

3.4. Cellulose biodegradability and its effect on cardiac cells

CA, with good characteristics from a manufacturing point of view (Fig. 1), is not easily degradable. However, partial hydrolysis and de-acetylization can reverse a pre-fabricated scaffold to a RC form, preserving the desired shape. In Fig. 6A, we summarize the outcome of several hydrolysis experiments, conducted to achieve the transition from CA to RC. After only 6 h of hydrolysis, the transition of CA to RC was documented by measuring the infrared spectra before and after treatment (Fig. 6B) using an FT-IR spectrophotometer Avatar 370. In agreement with previous studies [36], hydrolysis removed the peaks at 5.74, 7.3 and 8.2 μm characteristic for acetylated cellulose derivatives. Additionally, the 2.85 μm peak (presence of acetyl groups)

(A)

	Sample 1	Sample 2	Sample 3	Sample 4
Initial mass, mg	167	345	151	239
Hydrolysis Conditions t°C, time [h]	25°C, 6 h	25°C, 24 h	60°C, 6 h	60°C, 24 h
Mass loss, mg	55	136	62	102
Mass loss, %	33%	39%	41%	43%
Cellulase Treatment				
Mass loss, mg	18	15	20	30
Mass loss, %	16%	7%	23%	22%
Mass loss, mg/day	0.7	0.3	0.9	0.9
Released glucose, g/l	0.676	0.614	0.757	0.961
Released glucose, g/l/day	0.028	0.026	0.032	0.040

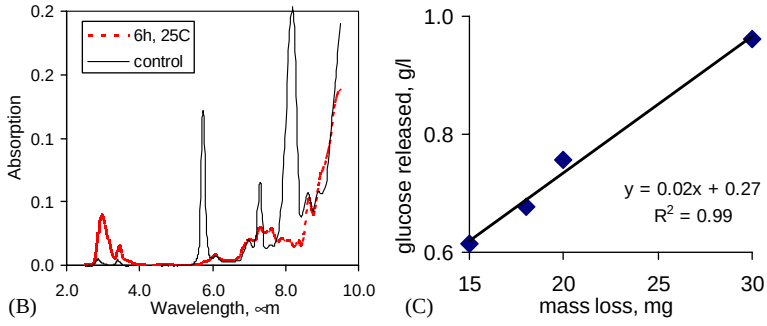

Fig. 6. CA scaffold biodegradability: (A) The table shows hydrolysis conditions and cellulase treatment (24 days, 70 units, at 37°C, pH 7.2) applied to 4 CA scaffolds. (B) IR-spectra were different for control and treated CA even after only 6 h of hydrolysis, indicating successful CA to RC conversion. (C) The CA degradation process was assessed by two alternative ways as loss of mass and released glucose with good correlation ($R^2 = 0.99$) between the two.

was substituted with a stronger peak at 3 μm, indicative of increase in OH^-. The hydrolysis step was followed by a slow enzymatic digestion step using cellulase. The action of the enzyme was probed by two alternative methods: loss of mass in the processed scaffolds, as well as the release of glucose in the solution assessed by a biochemical analyzer YSI 2700 Select (Yellow Springs Instruments, CA). The two measures of the degradation process showed high correlation ($R^2 = 0.99$), Fig. 6C.

The effect of cellulase was cell type specific, with the FB being more sensitive to the action of the enzyme than CM. Fig. 7 (left) shows representative fluorescence structural images of monolayers of cardiac fibroblasts after 24 h of cellulase treatment. FB adhesion to the surface was affected in a dose dependent manner (23, 46 and 92 enzyme units were used in Figs. 7A–C, respectively). This resulted in regional cell sheet detachment from the scaffold. CM, treated with the same cellulase concentrations, were much more resistant to detachment and showed no apparent differences from control samples in cytoskeletal structure and macroscopic cell organization (Fig. 7D). Cell viability, probed by Trypan Blue, was unaffected by the cellulase treatment. Nuclear images of control (Fig. 7F) and treated (Fig. 7E) cells showed similar cell densities.

4. Discussion and conclusions

In this study, we demonstrated that cellulose scaffolds are promoting cardiac cell growth, enhancing cell packing and connectivity, as well as electromechanical functionality, Figs. 2–5. Both, action potentials (the electrical triggers) and intracellular calcium (the mediator between the electrical and mechanical action) showed normal response to external stimulation. The cellulose-based materials exhibited better adhesion properties than most polymer surfaces, confirming earlier results with liver cells [8]. Our data reflect combined fibronectin and cell affinity and functionality when cellulose-based scaffolds are employed; no separate ECM protein adhesion tests were performed. Enhanced cell adhesion capacity and positive effects on the cell metabolism of cellulose surfaces have been linked to a particular component of the surface tension (indicator of material hydrophilicity/hydrophobicity) [8]. Another possible reason for CAs cytocompatibility could be the introduction of a polysaccharide microenvironment via the scaffold, consistent with the natural glycocalyx of the cell.

Cellulose-derived materials are well suited for further optimization and control of cell adhesion through

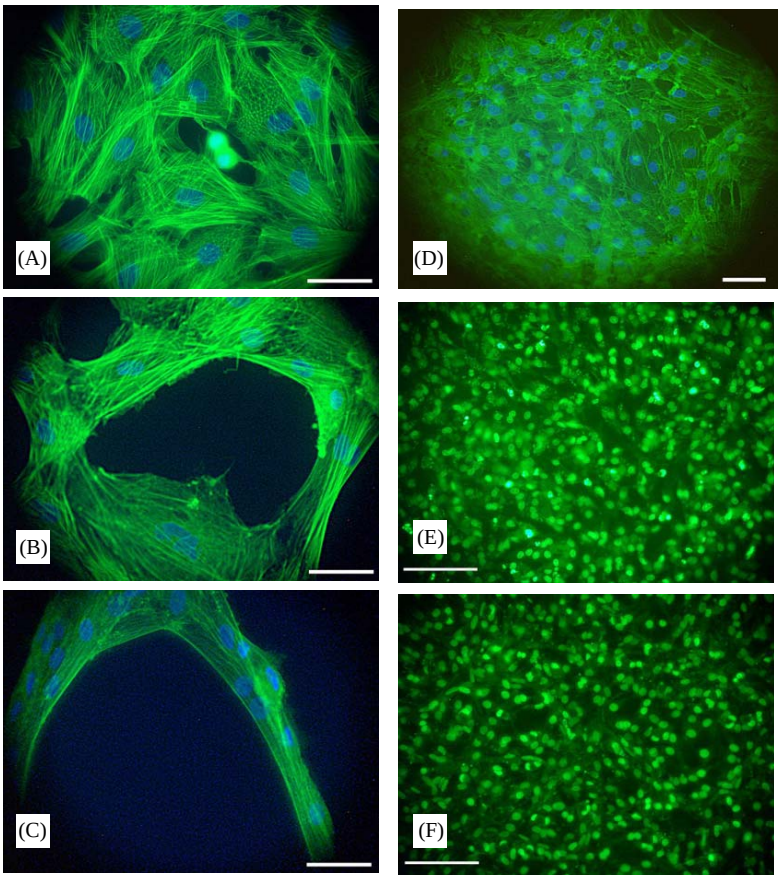

Fig. 7. Dose-dependent cellulase effects on cardiac cells: Cardiac fibroblasts were treated for 24 h with 23 units (A), 46 units (B) and 92 units (C) of cellulase, respectively. While at the lowest dose, a cell cytoskeleton was normal and undistinguishable from a control, at higher concentrations fibroblasts' adhesion to the matrix was affected, and cells were peeling off, forming empty holes. At the same time cardiac myocytes, treated with the same cellulase concentrations, preserved their macroscopic integrity at all doses. D shows a CM sample treated with 46 units for 24 h. Images (E) and (F) show live myocytes (nuclei labeled with SYTO-16) on cellulase-treated (92 units) and control sample, respectively. Scale bar is 50 μm (A-D) and 100 μm (E, F).

specific chemical surface modifications or through modifications to increase surface area. The former has been demonstrated before by functionalizing CA with an Arg-Gly-Asp (RGD)-peptide fused to the cellulose-binding domain (CBD) to augment cell attachment [16,37]. Surface area increase can be achieved using established methods for producing cellulose microfibers and textile-like matrices or using molding to introduce fine features (Fig. 1). Recently, electrospinning of CA was also demonstrated to obtain non-woven nanofibers [38]. Nanostructured scaffolds are believed to improve cellular response and biocompatibility [39]. CA rivals PDMS in its potential for easy construction of three-dimensional structures by casting/molding and extrusion. Well-controlled topographic features onto the biomaterial surface are important for achieving oriented cell growth to mimic the natural anisotropic characteristics of cardiac muscle [40]. In addition, cardiac muscle cells are known for their extremely high metabolic demands, yet they do not tolerate direct perfusion and high shear stress ($>1\,\mathrm{dyn/cm^2}$, [41]). Therefore, it is valuable to have the ability to embed tissue-compatible perfusion channels with semi-permeable walls for exchange of metabolites and with dimensions matching those of intermediate size blood vessels in the heart. Current commercially available hollow cellulose fibers match arteriole dimensions. These perfusion channels, needed exclusively in vitro during the tissuegenesis phase, can be easily incorporated in the cellulose scaffold and then completely degraded *prior* to implantation [18], thus facilitating the subsequent in-growth of blood vessels and perfusion of the implant.

For most in vitro applications of cardiac tissue equivalents, drug testing being one of them [42], biodegradability of the supporting scaffold structure is not a necessity. Nevertheless, we outline a strategy and provide preliminary data on cellulose biodegradability. The general resistance of most cellulose-based materials to natural degradation in physiological conditions could be used as an advantage by applying a tight control through cellulase availability (on/off) and dosage, since this enzyme is normally absent in mammals, yet

cytocompatible (based on our preliminary results). The final product of the cellulose degradation process is glucose—a natural nutrient for the cells, as contrasted to the acidic byproducts of the currently standard biodegradable PLGA scaffolds, for example. Cellulase treatment, in general, could be completely limited to pre-implantation to avoid possible adverse systemic reactions in vivo against the polymer or the enzyme. Further studies are needed to confirm in vivo applicability of cellulase and its effects on the heart muscle. Finally, unlike many other biomaterials, currently used for culturing cells—PLA/PGA, polyvinylchloride, Nylon, polystyrene, etc.—CA, being transparent and non-autofluorescent, allows the examination of cells by light and fluorescence microscopy.

5. Conclusion

In summary, we have demonstrated the use of cellulose scaffolds for growing structurally mature and functionally competent cardiac cell networks in culture. CA is a convenient starting polymer, which could be easily molded or otherwise modified to follow macro-, micro- and nanofeatures. If desired, CA could be treated post-shaping to RC for improved biodegradability. We conclude that in vitro growth of cardiac cells and tissue-like cardiac constructs for physiomics type of research could benefit from the versatility and accessibility of cellulose scaffolds; their use for tissue regeneration should also be considered.

Acknowledgements

This study was supported by research grants to EE from the Whitaker Foundation (RG-02-0654) and the American Heart Association (0430307N).

References

[1] Widmer MS, Gupta PK, Lu L, Meszlenyi RK, Evans GR, Brandt K, et al. Manufacture of porous biodegradable polymer conduits by an extrusion process for guided tissue regeneration. Biomaterials 1998;19(21):1945–55.

[2] Dar A, Shachar M, Leor J, Cohen S. Optimization of cardiac cell seeding and distribution in 3D porous alginate scaffolds. Biotechnol Bioeng 2002;80(3):305–12.

[3] Mikos AG, Sarakinos G, Leite SM, Vacanti JP, Langer R. Laminated three-dimensional biodegradable foams for use in tissue engineering. Biomaterials 1993;14(5):323–30.

[4] Boland ED, Bowlin GL, Simpson DG, Wnek GE. Electrospinning of tissue engineering scaffolds. Abstracts of Papers of the American Chemical Society 2001;222:31 (PMSE).

[5] Powers MJ, Domansky K, Kaazempur-Mofrad MR, Kalezi A, Capitano A, Upadhyaya A, et al. A microfabricated array bioreactor for perfused 3D liver culture. Biotechnol Bioeng 2002;78(3):257–69.

[6] Curtis ASG, Wilkinson CD. Reactions of cells to topography. J Biomater Sci-Polym Ed 1998;9(12):1313–29.

[7] Brunette DM, Chehroudi B. The effects of the surface topography of micromachined titanium substrata on cell behavior in vitro and in vivo. J Biomech Eng 1999;121(1):49–57.

[8] De Bartolo L, Morelli S, Bader A, Drioli E. Evaluation of cell behaviour related to physico-chemical properties of polymeric membranes to be used in bioartificial organs. Biomaterials 2002;23(12):2485–97.

[9] Miyamoto T, Takahashi S, Ito H, Inagaki H, Noishiki Y. Tissue biocompatibility of cellulose and its derivatives. J Biomed Mater Res 1989;23(1):125–33.

[10] Sevillano G, Rodriguez-Puyol M, Martos R, Duque I, Lamas S, Diez-Marques ML, et al. Cellulose acetate membrane improves some aspects of red blood cell function in haemodialysis patients. Nephrol Dial Transplant 1990;5(7):497–9.

[11] Burhop KE, Johnson RJ, Simpson J, Chenoweth DE, Borgia J. Biocompatibility of hemodialysis membranes: evaluation in an ovine model. J Lab Clin Med 1993;121(2):276–93.

[12] Chang Q, Murtaza Z, Lakowicz JR, Rao G. A fluorescence lifetime-based solid sensor for water. Anal Chim Acta 1997; 350(1–2):97–104.

[13] Kostov Y, Tzonkov S, Yotova L, Krysteva M. Membranes for optical Ph sensors. Anal Chim Acta 1993;280(1):15–9.

[14] Entcheva EG, Yotova LK. Analytical application of membranes with covalently bound glucose-oxidase. Anal Chim Acta 1994;299(2):171–7.

[15] Desai SD, Blanchard J. In vitro evaluation of pluronic F127-based controlled-release ocular delivery systems for pilocarpine. J Pharm Sci 1998;87(2):226–30.

[16] Doheny JG, Jervis EJ, Guarna MM, Humphries RK, Warren RAJ, Kilburn DG. Cellulose as an inert matrix for presenting cytokines to target cells: production and properties of a stem cell factor—cellulose-binding domain fusion protein. Biochem J 1999;339:429–34.

[17] Sardonini C, DiBiasio D. Design and operating criteria for hollow fiber bioreactors. Bioprocess Eng 1996;15(6):327–30.

[18] Ko IK, Iwata H. An approach to constructing three-dimensional tissue. Bioartif Org Iii: Tissue Sourcing, Immunoisolation, Clin Trials 2001;944:443–55.

[19] Katoh R, Urist MR. Surface-adhesion and attachment factors in bone morphogenetic protein-induced chondrogenesis in-vitro. Clin Orthop Rel Res 1993;(295):295–304.

[20] Martson M, Viljanto J, Hurme T, Saukko P. Biocompatibility of cellulose sponge with bone. Eur Surg Res 1998;30(6):426–32.

[21] Takata T, Wang HL, Miyauchi M. Migration of osteoblastic cells on various guided bone regeneration membranes. Clin Oral Implants Res 2001;12(4):332–8.

[22] Kino Y, Sawa M, Kasai S, Mito M. Multiporous cellulose microcarrier for the development of a hybrid artificial liver using isolated hepatocytes. J Surg Res 1998;79(1):71–6.

[23] Yang MB, Vacanti JP, Ingber DE. Hollow fibers for hepatocyte encapsulation and transplantation—studies of survival and function in rats. Cell Transplant 1994;3(5):373–85.

[24] Risbud MV, Bhonde RR. Suitability of cellulose molecular dialysis membrane for bioartificial pancreas: in vitro biocompatibility studies. J Biomed Mater Res 2001;54(3):436–44.

[25] LaIuppa JA, McAdams TA, Papoutsakis ET, Miller WM. Culture materials affect ex vivo expansion of hematopoietic progenitor cells. J Biomed Mater Res 1997;36(3):347–59.

[26] Cullen B, Watt PW, Lundqvist C, Silcock D, Schmidt RJ, Bogan D, et al. The role of oxidised regenerated cellulose/collagen in chronic wound repair and its potential mechanism of action. Int J Biochem Cell Biol 2002;34(12):1544–56.

[27] Ovington LG. Overview of matrix metalloprotease modulation and growth factor protection in wound healing. Part 1. Ostomy Wound Manage 2002;48(6 Suppl):3–7.
[28] Martson M, Viljanto J, Hurme T, Laippala P, Saukko P. Is cellulose sponge degradable or stable as implantation material? An in vivo subcutaneous study in the rat. Biomaterials 1999; 20(21):1989–95.
[29] Wang J, Hutchinskumar LD. Cellulose-acetate coated mercury film electrodes for anodic—stripping voltammetry. Anal Chem 1986;58(2):402–7.
[30] Entcheva E, Lu SN, Troppman RH, Sharma V, Tung L. Contact fluorescence imaging of reentry in monolayers of cultured neonatal rat ventricular myocytes. J Cardiovasc Electrophysiol 2000;11(6):665–76.
[31] Entcheva E, Bien H. Tension development and nuclear eccentricity in topographically controlled cardiac syncytium. J Biomed Microdev 2003;5(2):163–8.
[32] Vaija J, Lagaude A, Ghommidh C. Evaluation of image analysis and laser granulometry for microbial cell sizing. Antonie Van Leeuwenhoek 1995;67(2):139–49.
[33] Bien H, Yin L, Entcheva E. Cardiac cell networks on elastic microgrooved scaffolds. IEEE Eng Med Biol 2003;22(5):108–12.
[34] Saffitz JE, Green KG, Kraft WJ, Schechtman KB, Yamada KA. Effects of diminished expression of connexin43 on gap junction number and size in ventricular myocardium. Am J Physiol Heart Circ Physiol 2000;278(5):1662–70.
[35] Zhuang J, Yamada KA, Saffitz JE, Kleber AG. Pulsatile stretch remodels cell-to-cell communication in cultured myocytes. Circ Res 2000;87(4):316–22.
[36] Higgins HG, Stewart CM, Harrington KJ. Infrared spectra of cellulose and related polysaccharides. J Polym Sci 1961;51(155): 59–67.
[37] Wierzba A, Reichl U, Turner RFB, Warren RAJ, Kilburn DG. Adhesion of mammalian-cells to a recombinant attachment factor, Cbd/Rgd, analyzed by image-analysis. Biotechnol Bioeng 1995;46(3):185–93.
[38] Liu HQ, Hsieh YL. Ultrafine fibrous cellulose membranes from electrospinning of cellulose acetate. J Polym Sci Part B-Polym Phys 2002;40(18):2119–29.
[39] Matthews JA, Wnek GE, Simpson DG, Bowlin GL. Electrospinning of collagen nanofibers. Biomacromolecules 2002;3(2): 232–8.
[40] Streeter DD. Gross morphology and fiber geometry of the heart. In: Berne RM, Sperelakis N, Geiger SR, editors. Handbook of physiology, section 2: the cardiovascular system. Bethesda, MD: American Physiological Society; 1979. p. 61–107.
[41] Carrier RL, Rupnick M, Langer R, Schoen FJ, Freed LE, Vunjak-Novakovic G. Perfusion improves tissue architecture of engineered cardiac muscle. Tissue Eng 2002;8(2):175–88.
[42] Nave BT, Becker M, Roenicke V, Henkel T. Validation of targets and drug candidates in an engineered three-dimensional cardiac tissue model. Drug Discov Today 2002;7(7):419–25.